A Novel Austenite Aging Steel Laser Cladding Coating and Its Elevated-Temperature Wear Resistance

W. JIANG, L. WANG, and S.Q. WANG

A novel austenite aging steel coating was prepared by laser cladding to improve the elevated-temperature wear performance of AISI H13 steel. The wear tests at 400 °C to 600 °C were performed for the austenite aging steel coating and H13 steel. Their elevated-temperature wear performances were comparatively studied; the wear mechanisms under various loads at 400 °C to 600 °C were clarified. The novel austenite aging steel coating possessed an excellent elevated-temperature wear resistance. Comparatively, H13 steel presented an inferior wear resistance at 400 °C to 600 °C due to thermal softening, especially under a high load of 150 N at 600 °C. During elevated-temperature wear, a synergy of tribo-oxide layers and the subsurface matrix determined the wear behavior and mechanisms. Compared with H13 steel, higher resistance to thermal softening ensured a stable existence of the tribo-oxide layers owing to the precipitation strengthening of intermetallic compounds, thus endowing the austenite aging steel with the excellent elevated-temperature wear resistance. Consequently, for the novel austenite aging steel coating, oxidative mild wear prevailed at 400 °C to 600°C without the occurrence of the extrusive wear.

https://doi.org/10.1007/s11663-020-01839-3

I. INTRODUCTION

AISI H13 steel is widely used to make hot-working dies due to its high hot strength, toughness and thermal fatigue resistance.[1–4] One of its main failure modes is an elevated-temperature wear because of long-playing heating and sliding, which causes the variation of dimension and shape of the dies. Therefore, the dies fail prematurely, especially in severe working conditions.[2–6] However, the elevated-temperature wear performance (at 600°C or above) of H13 steel cannot be improved by heat treatment or microstructure variations. Hence, surface treatment would be an effective route to improve elevated-temperature wear performance of H13 steel.[6–8]

Laser cladding (LC) has obvious advantages over other surface treatment technologies: fine grains with rapid solidification characteristics, low dilution rate, small heat input and good metallurgical bond.[6,9,10] For laser cladding, laser energy is absorbed to melt cladding materials to form a coating on the surface of the substrate to improve its surface performance.[9] Clearly, the alloy composition of cladding materials is a key factor deciding the performance of the coating. Currently, for cladding materials, Fe-, Co- and Ni-based alloys were extensively studied and commercially applied to fabricate laser cladding coatings.[10–15] Compared with Co-based and Ni-based alloys,[11,12] Fe-based alloys were reported to have many merits of low cost, increased wear resistance and hardness.[10,13–15] Therefore, Fe-based alloys are suitable for the surface strengthening of ferrous alloys because of their full mutual solubility.

For most of Fe-based alloys, carbides are usually used as main strengthening phases to improve strength and wear resistance.[6,13–15] However, carbides readily coarsen at high temperatures to lose their reinforcing effect. Therefore, at high temperatures, Fe-based alloys would be thermally softened not to provide high deformation resistance and wear resistance. Rahmana *et al.* reported that the laser cladding HSS alloys possessed higher wear resistance at room temperature but experienced severe wear at 500 °C.[16] It may be considered that the inferior wear resistance of H13 steel is attributed to the above-mentioned thermal softening caused by the coarsening of carbides. Consequently, thermal softening (plastic deformation) and elevated-temperature wear might be a big obstacle for the application of hot-working dies made by H13 steel or Fe-based alloy coatings. In order to avoid the failures resulted from thermal

W. JIANG, L. WANG, and S.Q. WANG are with the School of Materials Science and Engineering, Jiangsu University, Zhenjiang 212013, China. Contact email: shuqi_wang@ujs.edu.cn
Manuscript submitted September 13, 2019.
Article published online April 10, 2020.

softening and elevated-temperature wear, the coarsening of strengthening phases at high temperatures should be retarded. Intermetallic compounds would be better substitutes for carbides as strengthening phases, just like maraging steel. Yin *et al.* found that the wear resistance performance of a maraging steel (18Ni-300) was improved after aging treatment because of precipitation strengthening.[17] Similarly for Stellite alloys, the addition of molybdenum was noticed to promote the precipitation of intermetallic compounds and improved the hardness and wear resistance.[18] However, the improvement of the precipitation of intermetallic compounds on elevated-temperature wear performance has been sparsely reported till now. For a Fe-based alloy, during elevated-temperature wear, intermetallic compounds as strengthening phases can enhance the hardness and resist thermal softening because of low diffusion coefficient. Hence, whether intermetallic compounds are able to improve elevated-temperature wear resistance needs to be further explored.

In the current research, a new-type austenite aging steel coating was produced on H13 steel by laser cladding. The austenite aging steel was developed based on a new composition design. It presented γ-(Fe, Ni) and intermetallic compounds as the matrix and the strengthening phases, respectively. The purpose of the research is mainly to explore the elevated-temperature wear resistance of this novel austenite aging steel coating, compared with H13 steel. Through investigating the morphology, composition and phases of worn surfaces and subsurfaces, the relationship of wear resistance with tribo-layers and substrate microstructures, and wear mechanisms were explored.

II. EXPERIMENTAL PROCEDURES

Based on the improvement of elevated-temperature wear performance, a novel austenite aging steel as the coating material was developed. The compositions of the novel Fe-based alloy coating are listed as follows (wt pct): 18 Ni, 5 Mo, 2.5 Cr, 0.2 Al, 2 Ti, and bal. Fe. Austenite-forming element Ni was used as main alloy element to form γ-(Fe, Ni) as matrix phase, and Ni, Mo, Al, and Ti were added to form intermetallic compounds. In addition, B and Si were used for deoxidation and slag formation.

The novel austenite aging steel coating was fabricated on the surface of the heat-treated H13 steel specimens with the dimensions of 30 mm × 30 mm × 15 mm. The multi-pass and multilayer methods were used to obtain the laser cladding coating by Nd^{3+}:YAG solid-state laser with argon gas shielding. Through optimization, the laser power and the scanning speed were selected to be 400 W and 5 mm/s, respectively, with the overlapping rate of 50 pct and the flow rate, 15 L/min of the protective gas argon. Prior to laser cladding, various raw powders were uniformly mixed by a planetary ball mill. The mixed powders were pasted on the substrate to form a preform of about 0.5 mm thick. During laser cladding, the laser beam was directed onto the surface of the preform to form a molten pool together with the melted H13 steel along the direction of laser movement. After the first layer was completed and cooled, a paste preform as the same as the first layer was covered and cladded to form the second layer in a vertical direction with the same parameters.

The heat-treated H13 steel was used as the comparative samples of wear tests and the laser cladding substrate. Commercial H13 steel was austenitized at 1020 °C for 30 minutes and oil cooled to obtain martensite and then was tempered at 600 °C for 2 hours to achieve tempered martensite with a hardness of 43 HRC. After laser cladding, the coating samples were treated by solid solution at 950 °C for 20 minutes and air cooled, subsequently aged at 600 °C for 2 hours to reach a hardness of 45 HRC. The heat-treated H13 steel and the coating samples were cut into pins by a line cutting with the sizes of 4.7 mm in diameter and 12.7 mm in height. M2 steel as counterface disks was austenitized at 1180 °C for 30 minutes and oil cooled, and then tempered three times at 540 °C for 2 hours, and air cooled to obtain tempered martensite with a hardness of 63 HRC. The nominal compositions of AISI H13 and M2 steels are listed in Table I. In order to evaluate the thermal softening resistance of heat-treated H13 steel and the coating, they were heated to 620 °C for 0.5, 1, 2, 5 and 8 hours, respectively, and then air cooled. The thermal softening resistance of H13 steel and the coating could be roughly estimated from the hardness variation as a function of the holding time. An HRS150 Rockwell hardness tester was used for Rockwell hardness measurement, which was performed five times at different positions on the sample surface to achieve the average value.

High-temperature wear tests were performed on a MMU-5GA friction and wear tester with the following parameters: temperatures of 400 °C, 500 °C and 600 °C, loads of 50, 100 and 150 N, sliding speed of 100 r/min, and sliding time of 20 minutes. The end surfaces of the pins and disks were polished by sandpapers to reach a roughness of 0.38 and 0.30 μm, respectively. After each wear test, the wear loss of each pin was measured by an E180 electronic analytical balance with an accuracy of 0.01 mg. For each test point, the wear test was repeated three times to obtain a mean value of wear loss. The wear rate was calculated by the formula: $W = \Delta M/\rho L$, where ΔM is the wear loss of a pin, ρ is the density of H13 steel and the coating material, respectively, and L is the sliding distance. A KB30S-FA type Vickers microhardness test system was used to determine the microhardness of worn subsurfaces with a force of 100 g and a dwell time of 15 seconds. The measurement for each point was repeated five times to achieve an average value and an error. The microstructure and phases of the coating were examined by a FEI Nova Nano 450 scanning electron microscopy (SEM) and a D/Max-2500/pc type XRD with Cu Ka radiation. A Kratos Axis Ultra DLD X-ray photoelectron spectroscopy (XPS) was applied to identify trace intermetallic compounds of the coating. For XPS analysis, a charge calibration must be performed for the original data according to the reference binding energy of C 1s peak (284.8 eV). The binding energy of the C 1s peak in

Table I. Nominal Compositions of AISI H13 and M2 Steels (Wt Pct)

Steel	C	Mn	Si	Cr	Mo	V	W	S	P	Fe
H13	0.46	0.32	1.04	5.31	1.45	1.38	—	≤ 0.03	≤ 0.03	bal.
M2	0.96	0.35	0.41	4.21	4.97	2.15	6.72	≤ 0.03	≤ 0.03	bal.

this experiment was noticed to be 284.9 eV, so the original data should be reduced by 0.1 eV. The filtering process was performed using Savitzky–Golay method. Finally, the calibrated binding energy and filtered data were used to fit in XPSpeak software. The morphology and phases of the worn surfaces of pins were investigated by using SEM and XRD, respectively. A DXR type laser Raman spectrometer (Raman) was used to detect trace oxides on worn surfaces with the laser wavelength of 532 nm and the power of 2 mW. Before the measure, the test sample was cleaned with acetone, and then was stuck on a glass slide with the worn surface facing up, and placed on an observation platform. In order to further examine the tribo-layers, the cross-sectional specimens of the worn surfaces for pins were prepared by a standard procedure with etching by aqua regia for 5 to 10 seconds. at room temperature.

III. RESULTS AND ANALYSIS

A. *Characterization of the Austenite Aging Steel Coating*

Figure 1 illustrates the microstructure of the austenite aging steel coating. As shown in Figure 1(a), a continuous and uniform coating was noticed to form on the H13 steel. The coating presented no crack and pore, as well as a good metallurgical bond with the H13 steel. The coating comprised the first layer (formed after the first laser cladding), the second layer (formed after the second laser cladding) and the remelting zone between the first and the second layers (Figures 1(b) and (c)). As shown in Figures 1(d) and (e), from the bottom to the top of the first layer, cellular crystals, columnar dendrites, equiaxed crystals and steering dendrites formed successively, as similar to the research.[19] The steering dendrites could be considered to be some columnar dendrites growing along the scanning direction.[15] Different from the microstructure of the first layer, the second layer almost presented columnar dendrites (Figure 1(b)), and the remelting zone between the two layers contained relatively coarse columnar dendrites (Figure 1(c)).

Figure 2 shows the XRD patterns of the austenite aging steel coating. The peaks of γ-(Fe, Ni), α-Fe and Ni_3Fe were noticed. Clearly, the matrix phase of the coating was γ-(Fe, Ni) with a small amount of α-Fe. The peaks of Ni_3Fe might overlay the ones of γ-(Fe, Ni). Therefore, Ni_3Fe could be considered to form in the coating to strengthen the matrix of the coating. However, for other precipitated intermetallic compounds, XRD could not identify their existence because of trace amount. According to the composition of the coating, intermetallic compounds of Ni-Al, Al-Fe *etc*. would be formed. In the present study, XPS analysis was used to identify trace intermetallic compounds (Figure 3). The high-resolution spectroscopies of Ni and Al are illustrated in Figures 3(a) and (b), respectively. Ni 2p peak consisted of one peak at the binding energy of 852.65 eV, corresponding to Al_3Ni (Figure 3(a)).[20] The binding states of Al in the coating were AlNi and Fe_3Al, the corresponding peaks were at the binding energy of 67.67 and 74.6 eV, respectively.[20,21] Based on the analysis of XRD and XPS patterns, intermetallic compounds Ni_3Fe, Al_3Ni, AlNi and Fe_3Al might precipitate in the coating.

B. *Tribological Performance of the Coating and H13 Steel*

Figure 4 illustrates the wear rates of H13 steel and the austenite aging steel coating under various sliding conditions. When the load increased at 400 °C, the wear rate of H13 steel firstly increased from 5.2×10^{-6} to 8.1×10^{-6} mm^3/mm, then decreased to 6×10^{-6} mm^3/mm. Comparatively, the coating presented a lower, slightly increased wear rate (less than 3×10^{-6} mm^3/mm) with the increase of load. At 500 °C, the wear rate of H13 steel abruptly decreased to less than 6×10^{-6} mm^3/mm. On the contrary, the wear rate of the coating slightly increased to 3.9×10^{-6} mm^3/mm. As the ambient temperature reached 600 °C, the coating presented a slightly increased wear rate as a function of load, which merely approached 5×10^{-6} mm^3/mm under 150 N. However, the wear rate of H13 steel increased from 7.5×10^{-6} to 9.2×10^{-6} mm^3/mm with the increase from 50 to 100 N, but substantially increased to 33×10^{-6} mm^3/mm under 150 N. Clearly, at 400 to 600 °C, the coating presented a higher wear resistance than H13 steel, especially at 600 °C and 150 N.

Table II summarizes the friction coefficients of H13 steel and the austenite aging steel coating under various sliding conditions. At 400 °C and 500 °C, the average friction coefficients of H13 steel and the coating decreased with the increase of load. At 600 °C, the average friction coefficient of the coating also decreased with the increase of load, while that of H13 steel absolutely increased. At 400 °C, H13 steel presented lower average friction coefficients than the coating under the corresponding loads. Conversely, at 500 °C and 600 °C, the coating possessed lower average friction coefficients than H13 steel. Overall, compared with H13 steel, the coating presented excellent tribological performance at elevated temperatures, especially at 500 °C and 600 °C.

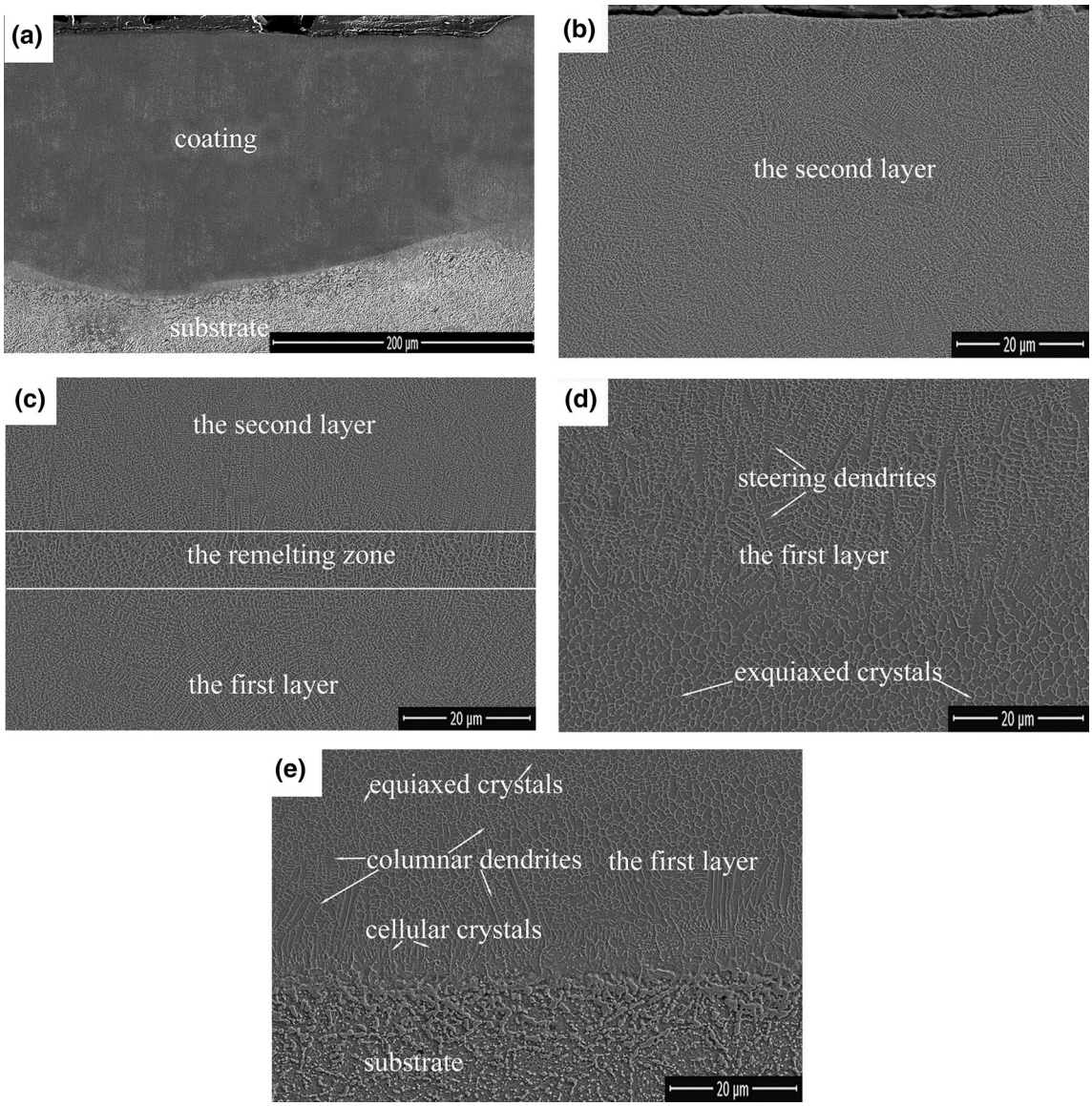

Fig. 1—SEM morphologies of the coating: the cross-sectional macro-morphology of the coating (*a*), the second layer (*b*), the remelting zone between the first and the second layer (*c*), the middle region of the first layer (*d*), and the bottom region of the first layer (*e*).

C. *Microscopic Analysis for Worn Surfaces*

The XRD patterns and Raman curves of worn surfaces of H13 steel and the coating are shown in Figures 5 and 6, respectively. As shown in Figure 5, a small amount of Fe_2O_3 and Fe_3O_4 were noticed to form on worn surfaces of H13 steel at 400 °C. As the ambient temperature reached 600 °C, a great amount of Fe_2O_3 and Fe_3O_4 with trace FeO (shown in Figure 6(a)) were produced on the worn surfaces. However, at 400 °C, a small amount of Fe_3O_4 were merely identified on worn surfaces of the coating. As the ambient temperature reached 600 °C, a great amount of Fe_3O_4 and a small amount of Fe_2O_3 were distinguished to appear on the worn surfaces of the coating. In addition, FeO and NiO were also identified in the Raman curves, as shown in Figure 6(b). Since the coating contained more anti-oxidation elements, such as Cr and Ni, its tribo-oxides seemed to be much less than those of H13 steel.

Figure 7 illustrates SEM morphology of the worn surfaces of H13 steel and the coating under various sliding conditions. It was found in Figure 5 that tribo-oxides started to appear on worn surfaces of H13 steel at 400 °C. When the ambient temperature reached 600 °C, the amount of tribo-oxides substantially increased. At 400 °C, the worn surface of H13 steel represented typical characteristics of oxidative wear with smooth, black areas (tribo-oxide layers) and rough, gray areas (delamination of tribo-oxide layers) (Figure 7(a)). However, at 600 °C, the worn morphology became different; smooth, black areas with cracks covered the

whole worn surface, as shown in Figure 7(b). It might be estimated that tribo-oxide layers would totally peel off for further sliding. For the coating at 400 °C to 600 °C, smooth, black areas, some rough delaminated areas and particles appeared on the worn surfaces (Figures 7(c) and (d)). As the ambient temperature increased to 600 °C, more and more particles appeared on worn surfaces (Figure 7(d)). Figure 8 illustrates the macro-morphology of worn specimens of H13 steel and the coating under 150 N at 600 °C. It was noticed that the pins of H13 steel and the coating almost maintained their original contours under most sliding conditions. Figure 8(b) presented not only the macro-morphology of the coating under 150 N at 600 °C, but also typical one of the coating and H13 steel in other sliding conditions. However, as H13 steel slid under 150 N at 600 °C, the worn specimen lost its original contour with the appearance of a plastically extrusive lip on the worn surface, as shown in Figure 8(a). It is clear that a severe wear occurred for H13 steel under 150 N at 600 °C. Conversely, the coating presented mild wear in the same condition.

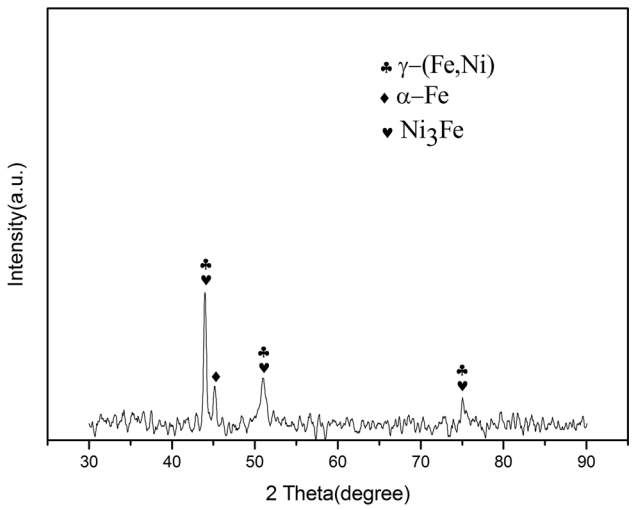

Fig. 2—XRD spectrum analysis of the cladding coating.

IV. DISCUSSION

Mild and severe wear is a relative concept, which is usually used to distinguish the wear severity.[22] Zhang and Alpas suggested 5×10^{-6} mm^3/mm as a critical value for mild wear.[23] In our current research, 5×10^{-6} mm^3/mm might as well use as a standard to evaluate the wear resistance of H13 steel and the coating. Mild and severe wear could be classified according to the wear rates below and above 5×10^{-6} mm^3/mm, respectively. As shown in Figure 4, the wear rate of H13 steel was less than 5×10^{-6} mm^3/mm under 50 N at 400 °C. As the load increased to 100 and 150 N, the wear rates surpassed 5×10^{-6} mm^3/mm. As the ambient temperature reached 500 °C, the wear rates slightly decreased to less than 5×10^{-6} mm^3/mm under 50 and 100 N, but surpassed 5×10^{-6} mm^3/mm under 150 N. However, as the ambient temperature reached 600 °C, the wear rates substantially increased to 7.1 to 8.7 $\times 10^{-6}$ mm^3/mm under 50 to 100 N, especially reached 33×10^{-6} mm^3/mm under 150 N. This demonstrated that the wear performance of H13 steel would be readily deteriorated at 400 °C and 600 °C, especially at 600 °C and 150 N.

When H13 steel was applied at 400 °C to 600°C, the wear rate readily surpassed the critical value of mild wear to enter severe wear. Therefore, H13 steel possessed unstable, inferior elevated-temperature wear resistance at 400 °C to 600 °C. It is unstandable that the hot-working dies made of H13 steel usually present normal or low life of wear. Furthermore, such dies would fail immediately as the temperature and load reached 600 °C and 150 N or above at local areas. By contrast, the wear rates of the coating were less than 4×10^{-6} mm^3/mm at 400 °C and 500 °C. Even at 600 °C and 150 N, the wear rate merely approached 5×10^{-6} mm^3/mm. Clearly, the coating invariably fell in mild wear

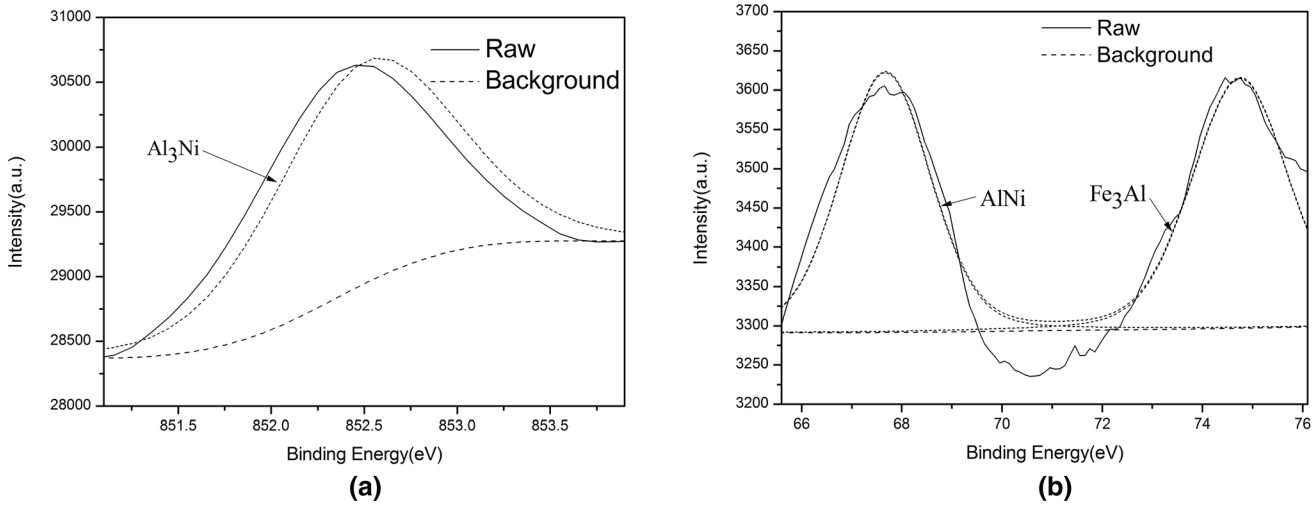

Fig. 3—XPS spectra of the coating surface : Ni 2p (*a*), and Al 2p (*b*).

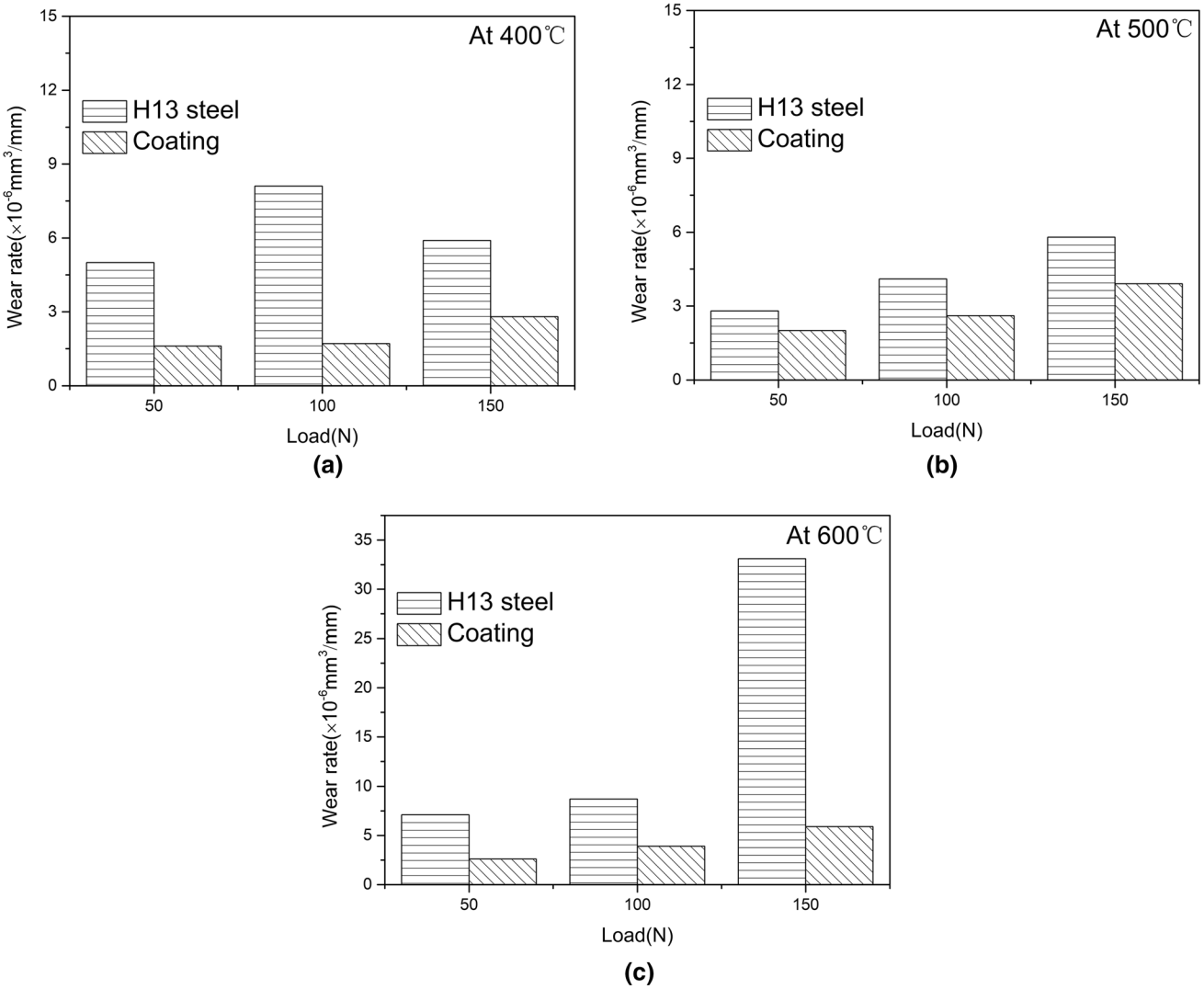

Fig. 4—Wear rates of H13 steel and the coating under various sliding conditions: 400 °C (*a*), 500 °C (*b*) and 600 °C (*c*).

under 50 to 150 N at 400 °C to 600 °C. This demonstrated that the austenite aging steel possessed excellent wear resistance, and was qualified for the coating on H13 steel. When this austenite aging steel coating was produced on H13 steel, the corresponding hot-working dies would be expected to possess a longer life of wear than the original ones.

During elevated-temperature wear of metallic alloys, tribo-oxides are unavoidably formed on worn surfaces. Tribo-oxides as the third body are bound to affect wear behavior and mechanism of metallic alloys.[24] Usually, tribo-oxides are considered to protect metallic alloys to reduce wear, while main wear mechanism is oxidative mild wear.[25,26] However, a prerequisite for the above-mentioned protection and oxidative mild wear must be needed. Namely, the subsurface alloy possessed enough thermal strength and stability to support tribo-oxide layers.[22,25] In this case, the thermal softening did not occur in the subsurface matrix, so tribo-oxide layer was strongly supported to take a protective function. Otherwise, although tribo-oxides existed, their protective function would be totally lost. Therefore, oxidative mild wear could not be maintained but turned into extrusive wear.[25]

Figure 9 illustrates the cross-sectional morphology of worn surfaces of H13 steel and the coating under 150 N at 600 °C. From the cross-sectional morphology of worn surfaces, the tribo-oxide layers could be identified from the matrix. Based on the characteristics of tribo-oxide layers, the wear behavior and wear mechanism could be estimated. At 600 °C and 150 N, the tribo-oxide layer of the coating was noticed to stably exist with a thickness of 26 μm, as shown in Figure 9(b). It was considered that the tribo-oxide layer possessed the protective function because of no plastic deformation of the subsurface matrix and sound tribo-layer. In contrast, the tribo-oxide layers of H13 steel were fractured to peel off. In this case, the tribo-oxide layers did not provide the protective function. This would be confirmed from massively plastic deformation (plastic flow traces)

Table II. Friction Coefficients of H13 Steel and the Austenite Aging Steel Coating Under Various Sliding Conditions ($\bar{\mu}$-Average Friction Coefficient, σ-Standard Deviation)

Temperature (°C)	400			500			600		
Load (N)	50	100	150	50	100	150	50	100	150
H13									
$\bar{\mu}$	0.93	0.51	0.39	0.86	0.59	0.48	0.48	0.62	0.73
σ	0.18	0.15	0.14	0.16	0.14	0.15	0.11	0.10	0.26
Coating									
$\bar{\mu}$	0.96	0.70	0.64	0.64	0.58	0.37	0.47	0.40	0.29
σ	0.20	0.16	0.16	0.14	0.17	0.14	0.16	0.09	0.11

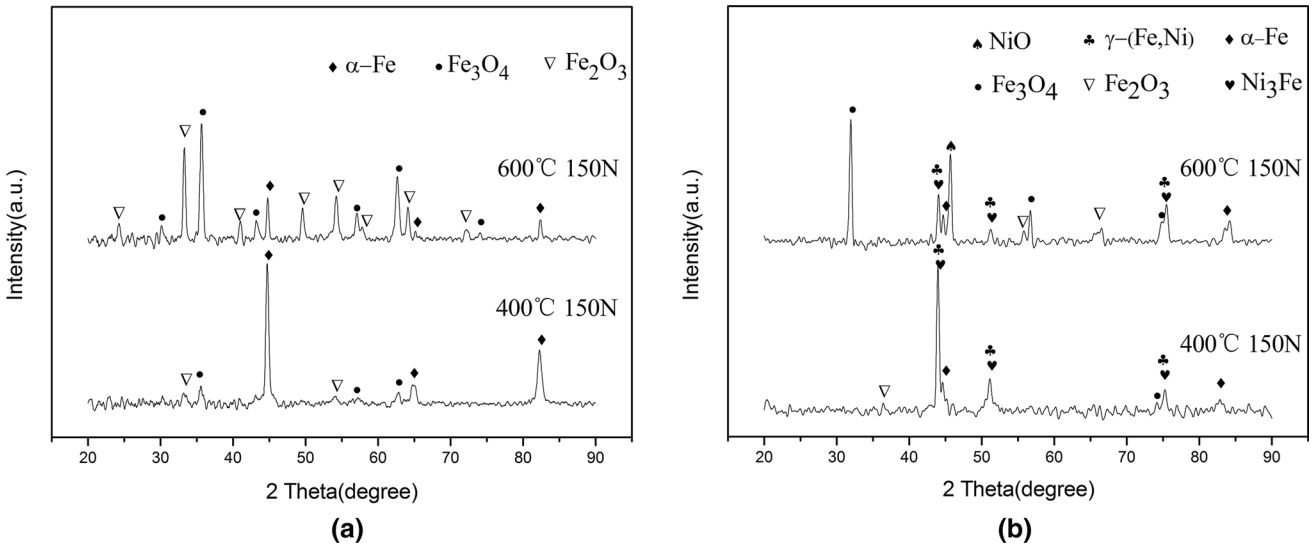

Fig. 5—XRD patterns of worn surfaces of H13 steel (*a*) and the coating (*b*).

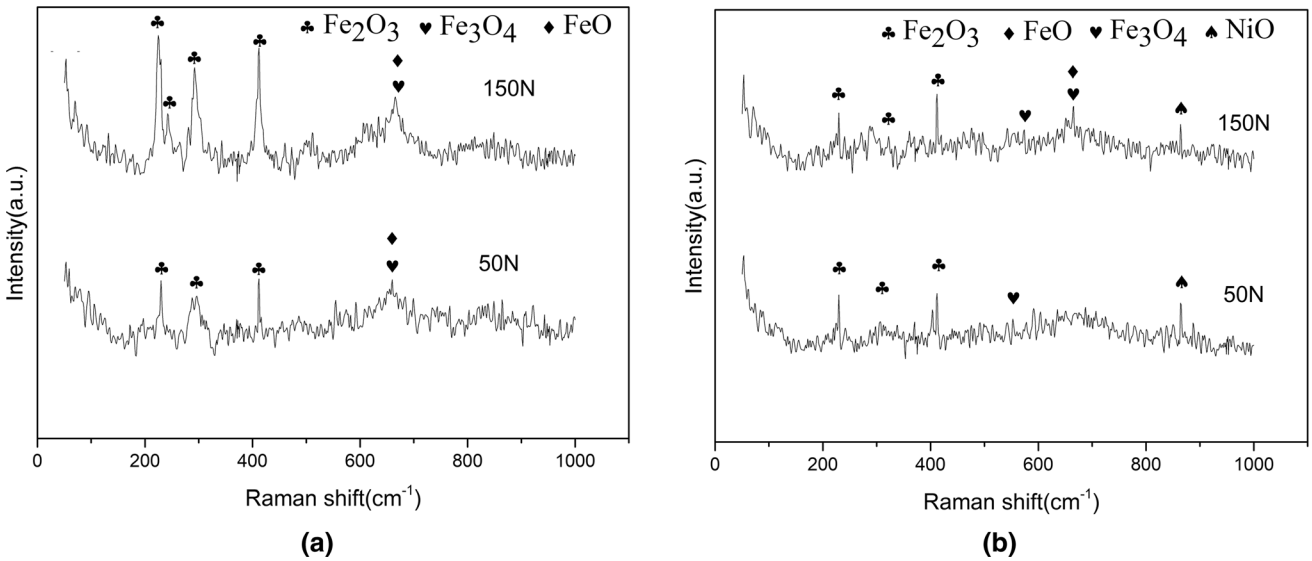

Fig. 6—Raman spectrum of worn surfaces for H13 steel (*a*) and the coating (*b*) at 600 °C.

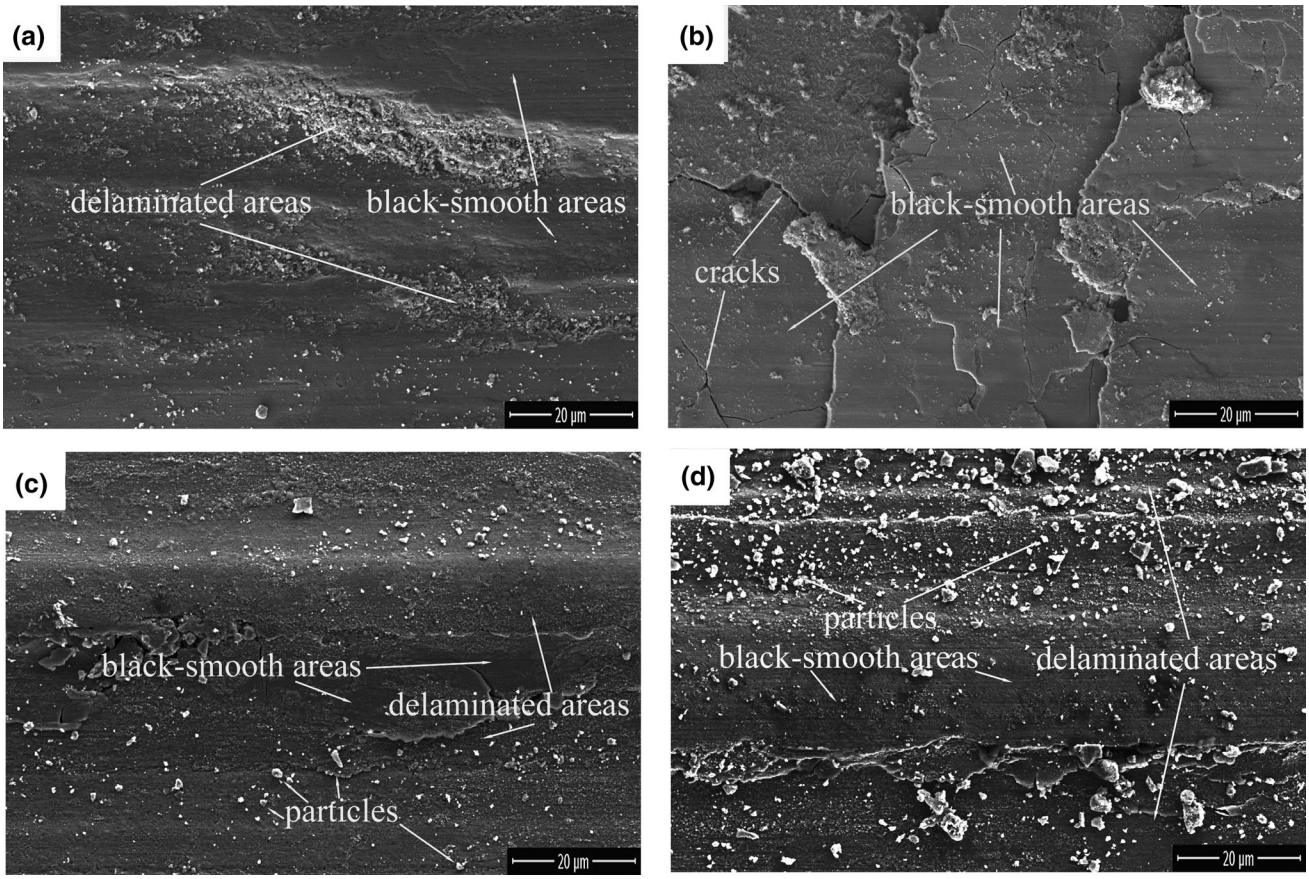

Fig. 7—SEM morphology of worn surfaces of H13 steel and the coating under various sliding conditions: H13 at 400 °C and 150 N (*a*), H13 at 600 °C and 150 N (*b*), the coating at 400 °C and 150 N (*c*), and the coating at 600 °C and 150 N (*d*).

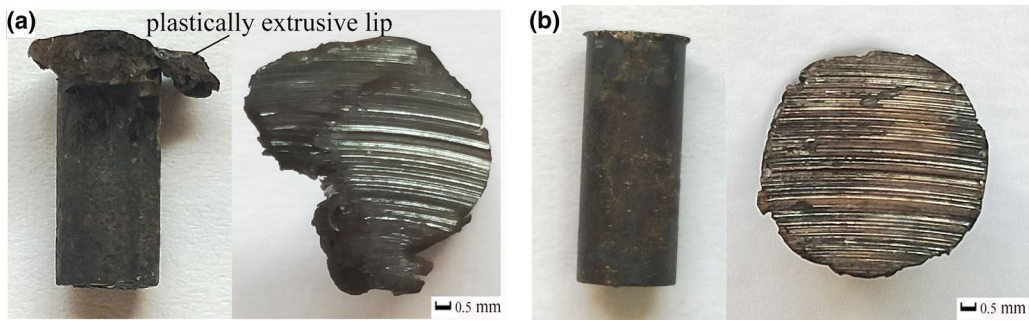

Fig. 8—Macro-morphology of worn specimens of H13 steel (*a*) and the coating (*b*) under 150 N at 600 °C.

occurred at subsurfaces, broken tribo-oxide layers and even the appearance of their double-layer structure (Figure 9(a)).

The protective function of tribo-oxide layers depended on the thermal strength and thermal stability of subsurface matrix. When subsurface matrix had enough thermal strength and thermal stability, tribo-oxide layers would be firmly supported to take a protection action. Conversely, as thermal strength and thermal stability of subsurface matrix were substantially reduced, tribo-oxide layers would lose the firm support not to take a protection action. In this case, massively plastic deformation occurred at subsurface matrix on account of no protection from tribo-oxide layers, thus resulting in their substantial delamination. The thermal strength and stability could be estimated by the resistance to thermal softening, *i.e.*, the hardness and its variation at an high ambient temperature. The resistance to thermal softening was considered to decide the elevated-temperature wear resistance.

For a hot-working die steel, thermal softening usually causes massively plastic deformation in elevated-temperature applications. More importantly, it severely damages elevated-temperature wear resistance.[25–27] In the present research, thermal softening extent would be roughly estimated by measuring the hardness variation

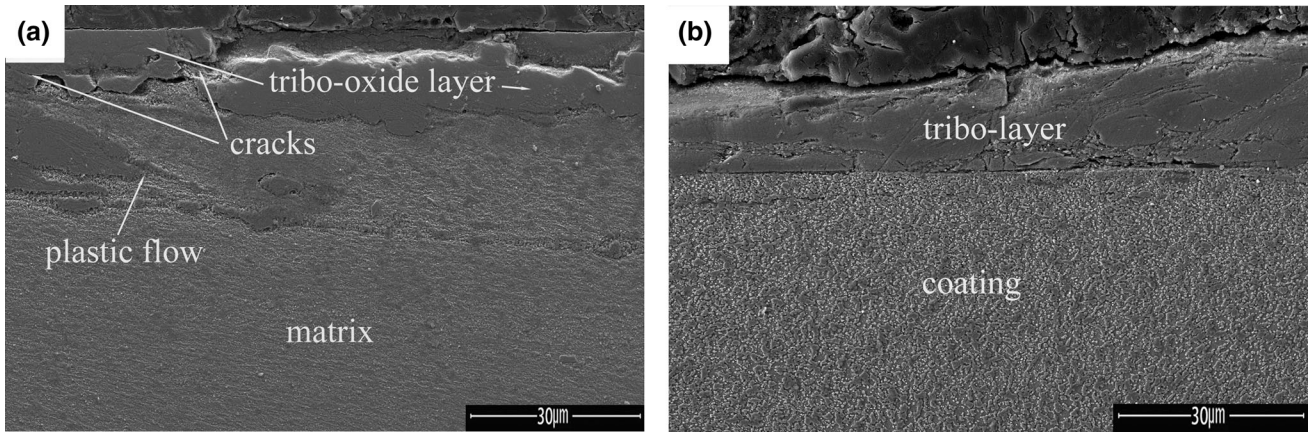

Fig. 9—Cross-sectional morphology of worn surfaces of H13 steel (*a*) and the coating (*b*) under 150 N at 600 °C.

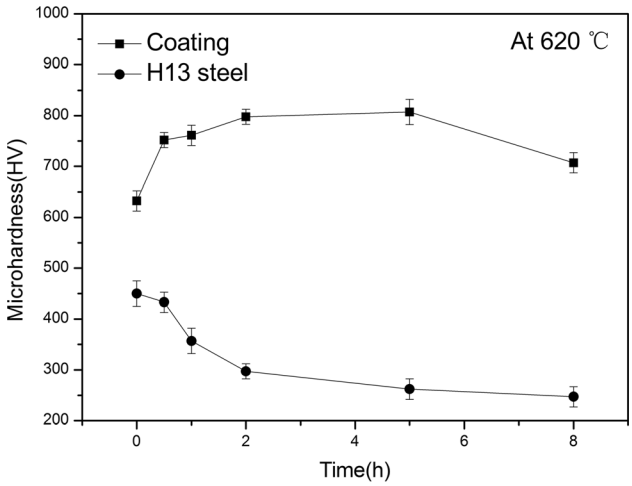

Fig. 10—Microhardness variation of H13 steel and the coating during the isothermal process at 620 °C.

after some durations at certain a high temperature. Figure 10 illustrates the hardness variation of H13 steel and the austenite aging steel coating after the same isothermal process at 620 °C. Because of the existence of intermetallic compounds, the austenite aging steel coating was hardened to reach 625 HV. With an increase of the holding time at 620 °C, the hardness of the austenite aging steel coating substantially increased to 800 HV after 5 hours, and then slightly decreased to 700 HV after 8 hours. Clearly, during elevated-temperature, the austenite aging steel coating was further strengthened by the continuous precipitation of intermetallic compounds. Conversely, H13 steel would be further tempered and carbides readily coarsened in the same condition, thus its hardness was markedly reduced from 450 HV to 300 HV after 2 hours, and slightly decreased to 250 HV after 8 hours at 620 °C with the increase of the holding time. The above experimental result demonstrated that the austenite aging steel coating had higher thermal strength and stability than H13 steel. The higher thermal strength and stability endowed the coating with the higher elevated-temperature wear resistance.

During sliding of metal alloys at elevated-temperature, more tribo-oxides were formed on worn surfaces. During sliding at 400 °C to 600 °C, Fe_2O_3, Fe_3O_4, and FeO were noticed to exist on worn surfaces of H13 steel. This is agreement with Godet's research.[24] For the coating, because of high content of Cr and Ni, relatively less tribo-oxides of Fe_2O_3, Fe_3O_4, FeO, and NiO were produced at the same sliding conditions. The appearance of tribo-oxides was helpful to reduce the friction coefficients of H13 steel and the coating because of their lubricating action.[24] Under higher loads at 600 °C, the lower friction coefficients of the coating might be attributed to the sound tribo-oxide layers and the appearance of NiO.[28] Similarly, deteriorated tribological performance of H13 steel was ascribed to the damage of the sound tribo-oxide layers in the same condition. For example, double-layer tribo-oxide layers appeared, as shown in Figure 9(a).

The appearance of tribo-oxides roughly confirmed that oxidative-induced wear prevailed for H13 steel and the coating. Wang *et al.* suggested a classification of oxidative-induced wear into oxidative mild wear and oxidative wear, based on wear rate and wear characteristics.[27] Although oxidative mild wear and oxidative wear present the same oxidative characteristic, the latter is beyond mild wear. In the present research, the characteristics of oxidative-induced wear were shown from the phases and morphology of worn surfaces. Based on 5×10^{-6} mm^3/mm as the critical wear rate of mild wear, oxidative-induced wear could be subdivided.

For the coating, the wear rates invariably kept below 5.0×10^{-6} mm^3/mm throughout. Hence, oxidative mild wear prevailed at 400 °C to 600 °C. However, for H13 steel, oxidative mild wear merely prevailed under 50 N at 400 °C and under 50 to 100 N at 500 °C. Under 100 to 150 N at 400 °C, and 150 N at 500 °C as well as 50 to 100 N at 600 °C, oxidative wear occurred. When sliding under 150 N at 600 °C, H13 steel presented a special morphology of worn surfaces. That is, fractured tribo-oxide layers covered worn surfaces with the appearance of the plastic flow at subsurfaces and the plastically extrusive lip (Figure 8(a)). Clearly, massively plastic deformation occurred on worn surface and at

subsurface of H13 steel under 150 N at 600 °C. Although tribo-oxides still existed, they started to severely delaminate and lost the protection function. Hence, plastically extrusive wear prevailed.

V. CONCLUSIONS

(1) A novel austenite aging steel coating was successfully produced on the surface of AISI H13 steel by laser cladding. The coating presented no crack and pore as well as a metallurgical bond with H13 steel. The austenite aging steel coating took γ-(Fe, Ni) as main matrix phase with a small amount of α-Fe and precipitated intermetallic compounds.

(2) The austenite aging steel coating possessed excellent wear resistance at 400 °C to 600 °C. Comparatively, H13 presented an inferior wear resistance at 400 °C to 600 °C, especially under 150 N at 600 °C. Because of higher resistance to thermal softening of the coating, tribo-oxide layers stably existed to substantially reduce the wear rates.

(3) Oxidative mild wear was main wear mechanism for the coating at 400 °C to 600 °C.

However, oxidative mild wear prevailed for H13 steel only under 50 N at 400 °C and under 50 to 100 N at 500 °C. Oxidative wear occurred under 100 to 150 N at 400 °C and 150 N at 500 °C as well as 50 to 100 N at 600 °C. As load reached 150 N at 600 °C, extrusive wear prevailed.

ACKNOWLEDGMENTS

The authors are grateful to the financial support by the Natural Science Research Program of Jiangsu Higher Education Institutions (17KJB430030) and the Research and Innovation Project for College Graduates of Jiangsu Province (No. SJCX18-0725).

REFERENCES

1. R.M. Horn and R.O. Ritchie: *Metall. Trans. A*, 1978, vol. 9, pp. 1039–53.
2. S. Kheirandish and A. Noorian: *J. Iron Steel Res. Int.*, 2008, vol. 15, pp. 61–66.
3. L. Shuang, X. Wu, S. Chen, and J. Li: *J. Mater. Eng. Perform.*, 2016, vol. 25, pp. 2993–3006.
4. M.X. Wei, S.Q. Wang, Y.T. Zhao, and F. Wang: *Metall. Mater. Trans. A.*, 2011, vol. 42A, pp. 3106–14.
5. S. Chander and V. Chawla: *Mater. Today Proc.*, 2017, vol. 4, pp. 1147–57.
6. P. Kattire, S. Paul, R. Singh, and W.Y. Yan: *J. Manuf. Process.*, 2015, vol. 20, pp. 492–99.
7. G. Castro, A. Fernandez Vicente, and J. Cid: *Wear*, 2007, vol. 263, pp. 1375–85.
8. R. Rodríguez Baracaldo, J.A. Benito, E.S. Puchicabrera, and M.H. Staia: *Wear*, 2007, vol. 262, pp. 380–89.
9. L. Dubourg and J. Archambeault: *Surf. Coat. Technol.*, 2008, vol. 202, pp. 5863–69.
10. J. Zeisig, N. Schädlich, L. Giebeler, J. Sander, J. Eckertl, U. Kühn, and J. Hufenbach: *Wear*, 2017, vols. 382–383, pp. 107–12.
11. Y.P. Kathuria: *Surf. Coat. Technol.*, 2000, vol. 132, pp. 262–69.
12. M.A. Anjos, R. Vilar, R. Li, M.G. Ferreira, W.M. Steen, and K. Watkins: *Surf. Coat. Technol.*, 1995, vol. 70, pp. 235–42.
13. X.Y. Yang, X. Peng, J. Chen, and F.H. Wang: *Appl. Surf. Sci.*, 2007, vol. 253, pp. 4420–26.
14. Z.K. Fu, H.H. Ding, W.J. Wang, Q.Y. Liu, J. Guo, and M.H. Zhu: *Wear*, 2015, vols. 330–331, pp. 592–99.
15. K.Y. Luo, X. Xu, Z. Zhao, S.S. Zhao, Z.G. Cheng, and J.Z. Lu: *J. Mater. Process. Technol.*, 2019, vol. 263, pp. 50–58.
16. N. Ur Rahman, M.B. De Rooij, D.T.A. Matthews, G. Walmag, M. Sinnaevee, and G.R.B.E. Römera: *Tribol. Int.*, 2019, vol. 130, pp. 52–62.
17. S. Yin, C.Y. Chen, X.C. Yan, X.H. Feng, R. Jenkins, P. O'Reilly, M. Liu, H. Li, and R. Lupoi: *Addit. Manuf.*, 2018, vol. 353, pp. 32–40.
18. J.H. Yao, Y.P. Ding, R. Liu, Q.L. Zhang, and L. Wang: *Opt. Laser Technol.*, 2016, vol. 104, pp. 321–27.
19. I. Hemmati, V. Ocelík, and J.T.M.D. Hosson: *J. Mater. Sci.*, 2011, vol. 46, pp. 3405–14.
20. D. Zhang and D. Kong: *Appl. Surf. Sci.*, 2018, vol. 457, pp. 69–82.
21. X. Luo, Z. Yao, P. Zhang, and D. Gu: *J. Alloy Compd.*, 2018, vol. 755, pp. 41–54.
22. Y. Wang, T.Q. Lei, and J.J. Liu: *Wear*, 1999, vol. 231, pp. 1–11.
23. J. Zhang and A.T. Alpas: *Acta Mater.*, 1997, vol. 45, pp. 513–28.
24. M. Godet: *Wear*, 1984, vol. 100, pp. 437–52.
25. Q.Y. Zhang, K.M. Chen, L. Wang, X.H. Cui, and S.Q. Wang: *Tribol. Int.*, 2013, vol. 61, pp. 214–23.
26. H. So, H.M. Chen, and L.W. Chen: *Wear*, 2008, vol. 265, pp. 1142–48.
27. S.Q. Wang, L. Wang, Y.T. Zhao, Y. Sun, and Z.R. Yang: *Wear*, 2013, vol. 306, pp. 311–20.
28. Y. Yu, J. Zhou, S. Ren, L. Wang, B. Xin, and S. Cao: *Tribol. Int.*, 2016, vol. 104, pp. 321–27.